Available online at www.sciencedirect.com
SCIENCE DIRECT®
PERGAMON
International Journal of Heat and Mass Transfer 46 (2003) 4513–4525
International Journal of HEAT and MASS TRANSFER
www.elsevier.com/locate/ijhmt

Improvement of thermal characteristics of latent heat thermal energy storage units using carbon-fiber brushes: experiments and modeling

Jun Fukai *, Yuichi Hamada, Yoshio Morozumi, Osamu Miyatake

Department of Chemical Engineering, Kyushu University, 6-10-1 Hakozaki, Higashi-ku, Fukuoka 812-8581 Japan

Received 19 August 2002

Abstract

Brushes made of carbon fibers with a high thermal conductivity are inserted on the shell side of a heat exchanger to enhance the conductive heat transfer rates in phase change materials. The experimental results show that the brushes essentially improve the heat exchange rate during the charge and discharge processes even when the volume fractions of the fibers are about one percent. A three-dimensional model describing the heat transfer in the heat exchanger is numerically solved. The model predicts well the experimental outlet fluid temperatures and the local temperatures in the composite.

Keywords: Thermal energy storage; Thermal conductivity enhancement; Carbon fiber; Heat exchanger

1. Introduction

The development of efficient and cost effective thermal energy storage units is necessary for the utilization of solar energy, industrial waste heat, distributed generation waste heat and so on. Phase change materials (PCMs) attract attention as thermal energy storage materials because their energy densities are much higher than those using sensible heat [1].

The latent heat thermal energy storage units previously studied are roughly classified into two types. One is a capsule type [2–9] and the other is a shell-and-tube type [10–17]. If vacant spaces are not considered for relaxing the volume change of the PCMs, the packing ratio of PCM in the former is no more than 0.74 (the closest packing of spheres), while that in the latter is usually no less than 0.90. Thus, the shell-and-tube type is suitable for minimizing the volume of the thermal storage unit. However, the latter is inferior to the former regarding the heat transfer area between the PCM and the heat transfer fluid. This means that the shell-and-tube type hardly follows sudden changes in the load compared to the capsule type. To overcome this problem, extension of the heat transfer area and enhancement of the thermal conductivity using fins, honeycombs, porous media, fibers and so on may be useful. Actually, several researchers examined the efforts on fins [10–14] and honeycombs [10,15–17] in the shell-and-tube type. However, no other technique was applied to this type to the best of the authors' knowledge.

In this study, carbon-fiber brushes proposed by the authors [18] are used for enhancing the thermal conductivity of the PCMs. The feature of the brushes is that the volume fraction of the fibers is accurately and easily controlled. In the present experiments, carbon fibers with a thermal conductivity of 190 W/m K were shaped into radial brushes and inserted along the space on the shell side. The effect of the brushes on the thermal responses of the heat exchanger is experimentally and numerically investigated. A three-dimensional heat

* Corresponding author. Tel.: +81-92-642-3515; fax: +81-92-642-3519.
E-mail address: jfukai@chem-eng.kyushu-u.ac.jp (J. Fukai).

0017-9310/$ - see front matter
doi:10.1016/S0017-9310(03)00290-4

Nomenclature

A	constant representing temperature dependence of thermal conductivity (W/m K^2)
c_p	specific heat (J/kg K)
d_b	diameter of brush (m)
d_i, d_o	inner and outer diameter of tube (m)
h	heat transfer coefficient (W/m^2 K)
k	thermal conductivity (W/m K)
$\boldsymbol{k}$	thermal conductivity tensor (W/m K)
M	mass (kg)
n	coordinate normal to the boundary surface (m)
q	heat transfer rate (W)
r	radial distance (m)
s	coordinate along the center of the tube (m)
t	time (s)
t_{res}	residence time (s)
T	temperature (K)
u_h	mean fluid velocity (m/s)
X_{fa}	volume fraction of fibers in a brush
X_f	local volume fraction of fibers
ρ	density (kg/m^3)

Subscripts

0	initial
a	insulator
c	composite
ch	charge
dis	discharge
f	fiber
h	heat transfer fluid
in	inlet
liq	liquid
m	phase change material
out	outlet
p	parallel model
r	random model
s	series model
sol	solid
t	tube wall

transfer model on the basis of the simple model [19] is numerically solved. The calculated results are compared with the experiments to examine the capacity of the model. The effect of natural convection in the liquid phase is also discussed.

2. Experimental setup

Physical properties of the fibers and paraffin wax are shown in Table 1. Those of urethane foam as a heat insulator are also indicated because they are used for the numerical calculations described later. The apparent specific heat of the paraffin wax measured using a differential scanning calorimeter (DSC) is shown in Fig. 1. There are three peaks in the DSC curves. The two peaks in the range 20–35 °C are due to the phase transition of the solid phase. A peak in the range 40–53 °C is due to the solid–liquid phase change. The latter is utilized to store the thermal energy in the present study. The latent heat calculated from the DSC curve is 1.8×10^5 J/kg.

Fig. 2 shows the details of the heat exchanger. Copper tubes (8.0 mm ID×9.5 mm OD) with six paths and

Table 1
Physical properties

Carbon fiber	
Diameter	10 μm
Thermal conductivity	190 W/m K
Specific heat	1000 J/kg K
Density	2120 kg/m^3
Paraffin wax	
Thermal conductivity	0.21 W/m K in solid 0.12 W/m K in liquid
Density	900 kg/m^3 at 25 °C 780 kg/m^3 at 60 °C
Urethane form	
Thermal conductivity	0.03 W/m K
Specific heat	1100 J/kg K
Density	30 kg/m^3

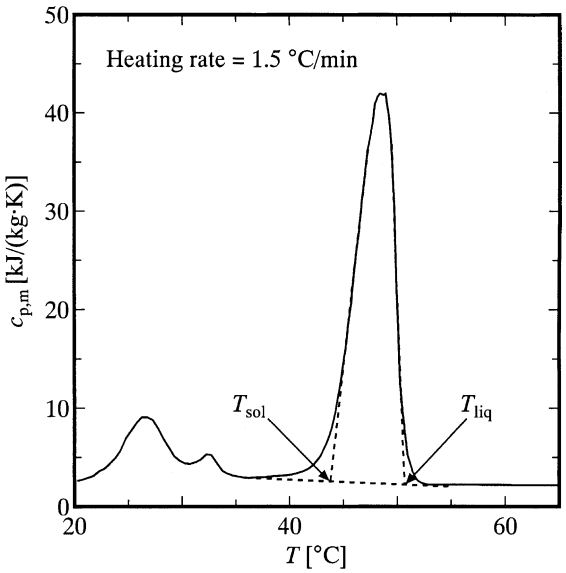

Fig. 1. Apparent specific heat of paraffin wax.

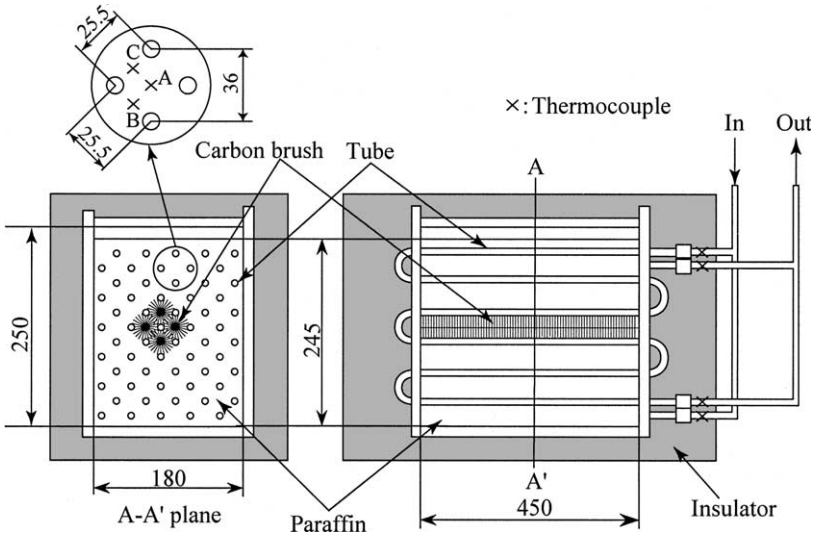

Fig. 2. The details of the thermal energy storage unit.

ten columns are arranged in a rectangular pitch. Water as the heat transfer fluid is on the tube side while paraffin wax as a PCM is on the shell side. The height of the PCM is 245 mm in the liquid state. The carbon-fiber brushes of 40-mm diameter and 450-mm length are inserted in the *whole* spaces among the tubes, though only a few brushes are drawn in the figure. It should be noted that the diameter of the brush is slightly larger than the tube pitch of 36 mm. The thermocouples are placed at the inlets and outlets of the tubes. Three thermocouples are placed near the upper surface of the PCM: one is at the center of four tubes, or the center of the brush, and two are in the middle of two tubes as shown in Fig. 2. Urethane foam encloses the heat exchanger.

High and low-temperature thermostatic baths were prepared. Water was provided from the former in the charge process, while it was provided from the latter in the discharge process. The fluid velocity was controlled and maintained at a constant.

The ratios of the fiber volume to the apparent volume of the brush, X_{fa}, were 0, 0.004 and 0.008. Overall, the volume ratio of the fibers to the brush/PCM composite in the unit is 0.0068 for $X_{fa} = 0.004$ and 0.0137 for $X_{fa} = 0.008$ because parts of the brushes are overlapped. The apparent thermal conductivities of the composites, including the thermal contact resistance between the fibers and the tube surfaces, are estimated to be 0.40 and 0.51 W/m K in the solid state [19], respectively. The two sets of the water temperature levels were examined: one was 55 °C (charge) −38 °C (discharge) and another was 60 °C (charge) −35 °C (discharge). The initial temperature in the unit was maintained at the water temperature in the discharge process. The mean fluid velocities of water were 0.015, 0.03 and 0.08 m/s.

3. Mathematical model

A three-dimensional heat transfer model in the storage unit is developed. The difficulties of the numerical calculations in this system result from the anisotropic heat transfer in the brush/PCM composite and the circular cross-section of the tubes. That is, many meshes are necessary to obtain the mesh-size independence solutions if they are accurately modeled. Fukai et al. [19] developed a simple model describing the two-dimensional heat transfer on the plane normal to the longitudinal direction of the tubes (the z–x plane in Fig. 3). They show that the simple model reduces the number of meshes to about 1/25 of a precise model. Accordingly, the simple model is extended to the three-dimensional model.

Assuming the adiabatic surfaces of the heat exchanger, the periodicity of the tube arrangement on the z–x plane reduces the computational domain as indicated by a dark area in Fig. 3(a). According to the simple model, the cross-sections of the tubes are assumed to be square. The side length of the outer tube wall is given by $\sqrt{\pi}d_o/2$ and that of the inner tube wall is given by $\pi d_i/4$.

The three-dimensional energy conservation equations in the brush/PCM composite (c), the tube wall (t) and the insulator (a) are given by

$$(c_p\rho)_c \frac{\partial T_c}{\partial t} = \nabla \cdot (\boldsymbol{k}_c \cdot \nabla T_c) \tag{1}$$

$$(c_p\rho)_t \frac{\partial T_t}{\partial t} = \nabla \cdot (k_t \nabla T_t) \tag{2}$$

$$(c_p\rho)_a \frac{\partial T_a}{\partial t} = \nabla \cdot (k_a \nabla T_a) \tag{3}$$

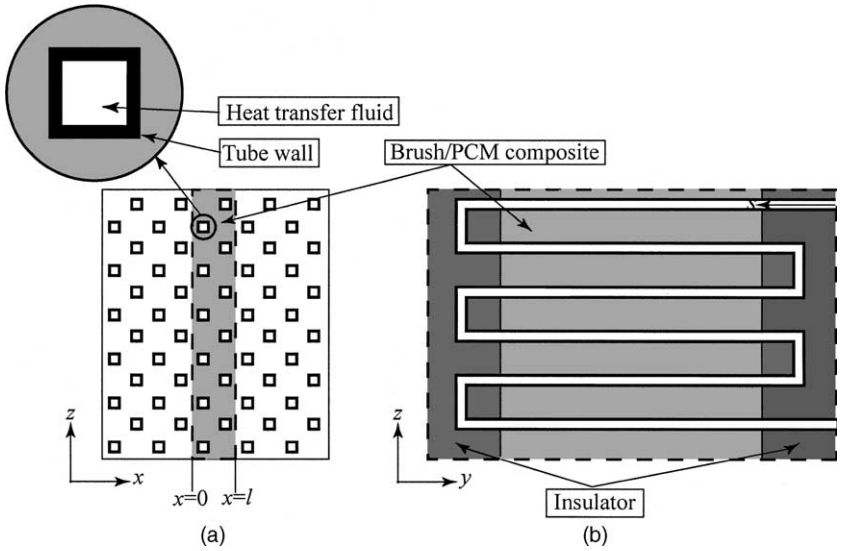

Fig. 3. Three-dimensional computational domain. (a) z–x plane and (b) y–z plane.

The convective heat transfer term does not appear in Eq. (1). Instead, its effect is considered in the thermal conductivity in the liquid phase as mentioned later.

For the heat transfer fluid (h), the following one-dimensional conservation equation is given by:

$$(c_p\rho)_{\mathrm{h}}\left(\frac{\partial T_{\mathrm{h}}}{\partial t}+u_{\mathrm{h}}\frac{\partial T_{\mathrm{h}}}{\partial s}\right)=\frac{\partial}{\partial s}\left(k_{\mathrm{h}}\frac{\partial T_{\mathrm{h}}}{\partial s}\right) \tag{4}$$

where s is the coordinate along the center of the tube measured from the inlet of the tube, u_{h} the mean fluid velocity, and T_{h} the bulk temperature of the fluid. In the present analysis, Eq. (4) is independently adopted to the heat transfer fluid flowing in the two tubes.

The initial conditions are

$$T_j=T_0 \quad \text{at } t=0 (j=c,t,h,a) \tag{5}$$

The boundary conditions are given by:

$$T_{\mathrm{h}}=T_{\mathrm{in}}(t) \text{ at the inlets of the tubes} \tag{6}$$

$$-k_{\mathrm{t}}\frac{\partial T_{\mathrm{t}}}{\partial n}=h_{\mathrm{h}}(T_{\mathrm{t}}-T_{\mathrm{h}}) \text{ on the tube-wall/fluid interface} \tag{7}$$

$$T_{\mathrm{c}}=T_{\mathrm{t}},\quad k_{\mathrm{c}}\frac{\partial T_{\mathrm{c}}}{\partial n}=k_{\mathrm{t}}\frac{\partial T_{\mathrm{t}}}{\partial n}$$
$$\text{on the composite/tube-wall interface} \tag{8}$$

$$T_{\mathrm{c}}=T_{\mathrm{a}},\quad k_{\mathrm{c}}\frac{\partial T_{\mathrm{c}}}{\partial n}=k_{\mathrm{a}}\frac{\partial T_{\mathrm{a}}}{\partial n}$$
$$\text{on the composite/insulator interface} \tag{9}$$

$$T_{\mathrm{t}}=T_{\mathrm{a}},\ k_{\mathrm{t}}\frac{\partial T_{\mathrm{t}}}{\partial n}=k_{\mathrm{a}}\frac{\partial T_{\mathrm{a}}}{\partial n} \text{ on the tube-wall/insulator interface} \tag{10}$$

$$-k_j\frac{\partial T_j}{\partial n}=0 \quad \text{on the outer boundary surface } (j=c,t,a) \tag{11}$$

$$T_j|_{x=0}=T_j|_{x=l},\quad k_j\left.\frac{\partial T_j}{\partial x}\right|_{x=0}=k_j\left.\frac{\partial T_j}{\partial x}\right|_{x=l}$$
$$\text{on the periodic surface } (j=c,a) \tag{12}$$

where n is the coordinate normal to the boundary surface, and h_{h} the heat transfer coefficient.

The heat capacity of the composite is given as a function of the local volume fraction of the fibers (X_{f}):

$$(\rho c_p)_{\mathrm{c}}=X_{\mathrm{f}}(\rho c_p)_{\mathrm{f}}+(1-X_{\mathrm{f}})(\rho c_p)_{\mathrm{m}} \tag{13}$$

In this equation, the apparent specific heat of the PCM, $c_{p,\mathrm{m}}$, is approximated by a polynomial function of the temperature based on the DSC curve shown in Fig. 1.

According to the simple model [19], the region of the composite is divided into four types of regions as shown in Fig. 4. The components of the thermal conductivity tensor are given with the combination of the modified parallel, series and random models:

$$k'_{\mathrm{p}}=0.3X_{\mathrm{f}}k_{\mathrm{f}}+(1-0.3X_{\mathrm{f}})k_{\mathrm{m}} \tag{14}$$

$$k'_{\mathrm{s}}=\{0.7X_{\mathrm{f}}/k_{\mathrm{f}}+(1-0.7X_{\mathrm{f}})/k_{\mathrm{m}}\}^{-1} \tag{15}$$

$$k'_r=0.456\{1-(1-0.1X_{\mathrm{f}})^{2/3}\}k_{\mathrm{f}}+(1-0.1X_{\mathrm{f}})^{1/3}k_{\mathrm{m}} \tag{16}$$

The asymmetric terms of $\boldsymbol{k}_{\mathrm{c}}$ in Eq. (1) vanish. k_{xx} and k_{zz} in the four regions are given by

$$k_{\mathrm{c},xx}=k'_{\mathrm{p}},\quad k_{c,zz}=k'_{\mathrm{p}} \text{ in region A} \tag{17}$$

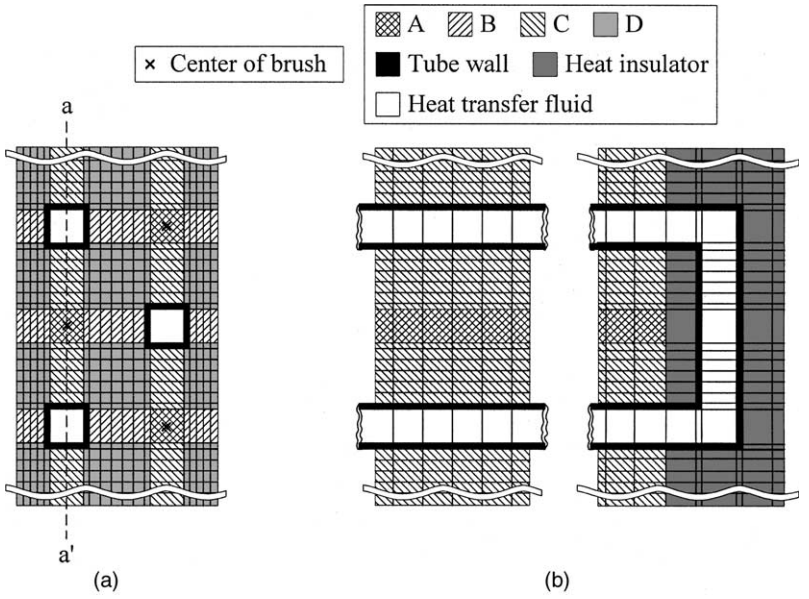

Fig. 4. The typical grids generated in the computation domain. (a) z–x plane and (b) y–z plane on a–a′.

$$k_{c,xx} = k'_p, \quad k_{c,zz} = k'_s \text{ in region B} \tag{18}$$

$$k_{c,xx} = k'_s, \quad k_{c,zz} = k'_p \text{ in region C} \tag{19}$$

$$k_{c,xx} = k'_r, \quad k_{c,zz} = k'_r \text{ in region D} \tag{20}$$

The constants in Eqs. (14)–(16) were determined for the simple model to accurately predict the heat transfer rate between the composite and the heat transfer fluid under wide conditions [19]. k_{yy} in all regions is represented by the well-known series model:

$$k_{yy} = \{X_f/k_f + (1 - X_f)/k_m\}^{-1} \tag{21}$$

X_f in the Eqs. (13)–(16) and (21) is approximated by [18]

$$X_f(r) = \begin{cases} 1 & \text{at } 0 \leqslant 2r/d_b \leqslant X_{fa}/2 \\ X_{fa} d_b/4r & \text{at } X_{fa}/2 < 2r/d_b \leqslant 1 \\ 0 & \text{at } 2r/d_b > 1 \end{cases} \tag{22}$$

where d_b is the diameter of the brush, and r the local radial distance from the center of the brush. Considering that a part of a brush overlaps other brushes, the local volume fraction of the fibers is generally calculated from the sum of the volume fraction for the ith brush, $X_{f,i}(r)$:

$$X_f = \sum_i X_{f,i}(r) \tag{23}$$

If the natural convective heat transfer in the liquid phase plays an important role, the apparent thermal conductivity in the liquid must be higher than the true value. However, a stepwise change in the thermal conductivity of the PCM results in numerical instability. Accordingly, the thermal conductivity of the PCM is assumed to increase continuously and lineally with temperature starting from T_{liq}:

$$k_m = \begin{cases} k_{m,sol} & \text{at } T < T_{sol} \\ \dfrac{k_{m,liq} - k_{m,sol}}{T_{liq} - T_{sol}}(T - T_{sol}) + k_{m,sol} & \text{at } T_{sol} \leqslant T \leqslant T_{liq} \\ A(T - T_{liq}) + k_{m,liq} & \text{at } T > T_{liq} \end{cases} \tag{24}$$

where T_{sol} and T_{liq} are the starting and ending temperatures of the melting, respectively, and A a constant representing temperature dependence of thermal conductivity. The values of $T_{sol} = 43.8$ and $T_{liq} = 50.6$ °C are chosen on the basis of the DSC curves in Fig. 1.

The governing equations are numerically solved using the control volume method [20]. Fig. 4 shows typical grids generated in the computational domain. On the z–x plane, the domain where the heat transfer fluid flows is fitted by a mesh. The meshes at both ends of the region D are placed so as to fit with the thickness of the tube wall. The region D is divided into 7×7 meshes, which are sufficient to provide the mesh-size independent solutions [19]. On the y–z plane, the tubes are assumed to form a right angle on both sides as shown Fig. 4(b). The typical number of meshes is $19 \times 45 \times 100$ and the time step is 5 s. The thermal storage/release energy from the unit is calculated from the difference between the inlet and outlet fluid temperatures. Another value is calculated from the time variation in the thermal energy within the computational domain. They agreed within 0.1% in each time step.

4. Results

4.1. Experimental

Fig. 5 compares the experimental heat exchange rates for different values of X_{fa}. The heat exchange rate is calculated by

$$q = (c_p\rho)_h u_h \left(\frac{\pi d_i^2}{4}\right)(T_{in} - T_{out}) \tag{25}$$

In the charge process, the natural convection in the liquid phase is well-known to play an important role in the enhancement of the heat transfer rate between the PCM and the tube surface. In spite of this fact, the heat exchange rate at the first half increases as X_{fa} increases (Fig. 5(a)). This fact shows that an increase in the effective thermal conductivity of the composite fully makes up for the reduction in the convective heat transfer rate. There is an irregular thermal response at 90–150 min for $X_{fa} = 0$. This is because lumps of the PCM are elevated in the liquid phase due to buoyancy and come into contact with the tube surfaces. However, the contact heat transfer dose not frequently occur at the earlier stage, resulting in low heat transfer rates for $X_{fa} = 0$. On the other hand, the thermal conductivity of the PCM directly affects the heat exchange rate in the discharge process because the solid phase develops from the tube surface. As a result, q at the first half essentially increases as X_{fa} increases.

The curves for $k_m = \infty$ are obtained by numerically solving the following equation:

$$\frac{d\{(M_m c_{p,m} + M_t c_{p,t})T(t - t_{res})\}}{dt} = (\rho c_p)_h \left(\frac{\pi d_i^2}{4}\right) u_h \{T(t - t_{res}) - T_{in}\} \quad \text{at } t > t_{res} \tag{26}$$

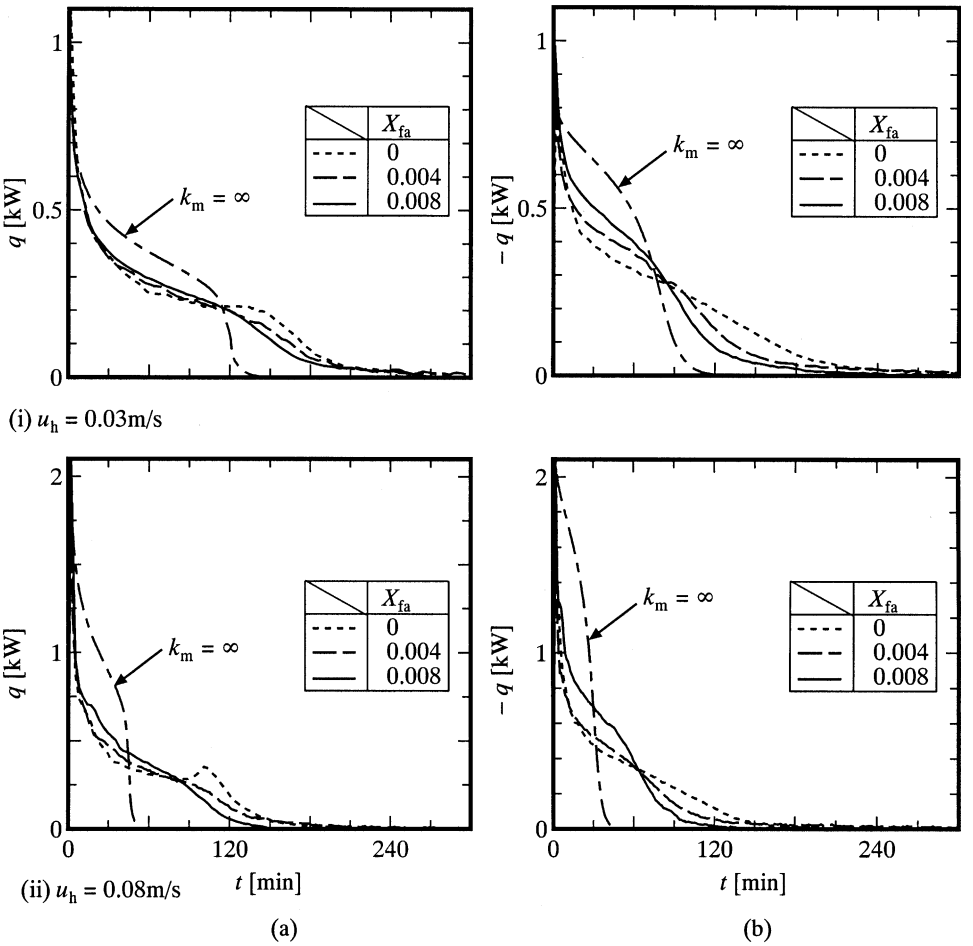

Fig. 5. The time variations in the experimental heat exchange rates. The effect of the brushes on the heat exchange rate (The fluid temperature = 55 °C in the charge −38 °C in the discharge). (a) Charge and (b) discharge.

where M is mass, and t_{res} the residence time of the fluid in the tubes. The results were numerically confirmed to agree with the three-dimensional model where k_m was assumed to be infinity. The effect of the brushes on the heat exchange rate in the charge and discharge processes is exemplified by the times, $t_{0.1}$, when the absolute value of q reaches 0.1 kW. $t_{0.1}$ normalized with the time for $k_m = \infty$ is shown in Table 2. The fibers with one percent reduce $t_{0.1}$ 10–20% in the charge process and about 30% in the discharge process.

Fig. 6 shows the time variations in the measured temperatures in the composite. For $X_{fa} = 0$ in the charge process, the temperature at point A suddenly rises from 47 °C to 53 °C due to the natural convection, resulting in little temperature difference in the PCM. Although there is no sudden change for $X_{fa} \neq 0$, the high conductive heat transfer rate reduces the times when the temperature reaches the water temperature. In the discharge process, the temperatures go down to 50 °C immediately after the energy releases due to the natural convection. However, the temperature differences in the PCM are larger than those for $X_{fa} \neq 0$ below 50 °C. The experimental results for $X_{fa} \neq 0$ show the characteristics of the heat transfer in the composite. That is, in the discharge process, the temperature at point A at $X_{fa} = 0$ is the lowest because this point is farther away from the tube surface than the others. However, the temperature at point A is the highest when $X_{fa} = 0.004$ and 0.008. The same results are observed in the charge process. This reverse of the temperature distribution results in the anisotropic conductive heat transfer in the composite [19].

4.2. Numerical

Figs. 7 and 8 show the dependence of the local temperatures and the outlet fluid temperatures on the A-value in Eq. (24) for $X_{fa} = 0$. In the charge process in Fig. 7, the calculated local temperatures for $A = 2$ and 10 W/m K^2 are much closer to the experimental than those for $A = 0$. As a result, the model predicts well the sudden change in the outlet fluid temperature at 220 min in Fig. 8 when the value of $A = 2$ or 10 W/m K^2 is assumed. In the discharge process, the calculated local temperatures for higher values of A also agree with the experimental values better than those for $A = 0$. However, the outlet fluid temperature is more insensitive to the A-value than that in the charge process because the conductive heat transfer rate in the solid phase dominates the overall heat transfer rate in the discharge process. The fact that there is little difference between the calculated results for $A = 2$ and 10 W/m K^2 probably shows that the apparent thermal conductivity in the liquid can be regarded as infinity due to the natural convection.

Figs. 9 and 10 show the time variations in the outlet fluid temperatures under all experimental conditions carried out in the present study. The calculated results for $A = 0$ and 2 W/m K^2 are indicated because there is little difference between the calculated results for $A = 2$ and 10 W/m K^2 as shown in Figs. 7 and 8. From a comparison between the experiments and calculations, it is again certain that the calculated results for $A = 2$ W/m K^2 are much closer than those for $A = 0$ W/m K^2 when $X_{fa} = 0$. Consequently, the present model can be applied to the case for $X_{fa} = 0$ by assuming a high thermal conductivity in the liquid phase.

Contrary to $X_{fa} = 0$, the difference between the calculated results for $A = 0$ and 2 W/m K^2 is small when $X_{fa} \neq 0$. However, in the charge process, the calculated outlet fluid temperatures for $A = 2$ W/m K^2 suddenly change starting from $T_{out} \approx 51$ °C though such a sudden change is not observed in the experiments. In other words, the calculations for $A = 0$ give better predictions than those for $A = 2$ W/m K^2. This fact shows that the fibers surely prevent natural convection in the liquid phase.

Consequently, the present models predict well the experimental thermal responses by assuming $A = 0$ for $X_{fa} \neq 0$ and a high value of A, e.g. >2 W/m K^2, for $X_{fa} = 0$.

Fig. 11 compares the calculated local temperature in the composite with the experimental values. The simple model has prediction errors to some degree for the local temperatures in the composite because the constants in Eqs. (14)–(16) are determined to accurately predict the heat exchange rate between the composite and the heat transfer fluid. However, this figure demonstrates that the

Table 2
Experimental time to be required for the absolute value of the heat exchange rate to reach 0.1 kW

u_h [m/s]	Charge			Discharge		
	$X_{fa} = 0$	$X_{fa} = 0.004$	$X_{fa} = 0.008$	$X_{fa} = 0$	$X_{fa} = 0.004$	$X_{fa} = 0.008$
0.03	1.45	1.37	1.26	1.79	1.44	1.28
0.08	2.85	2.62	2.32	3.38	2.70	2.32

The results are normalized with the time for $k_m = \infty$.

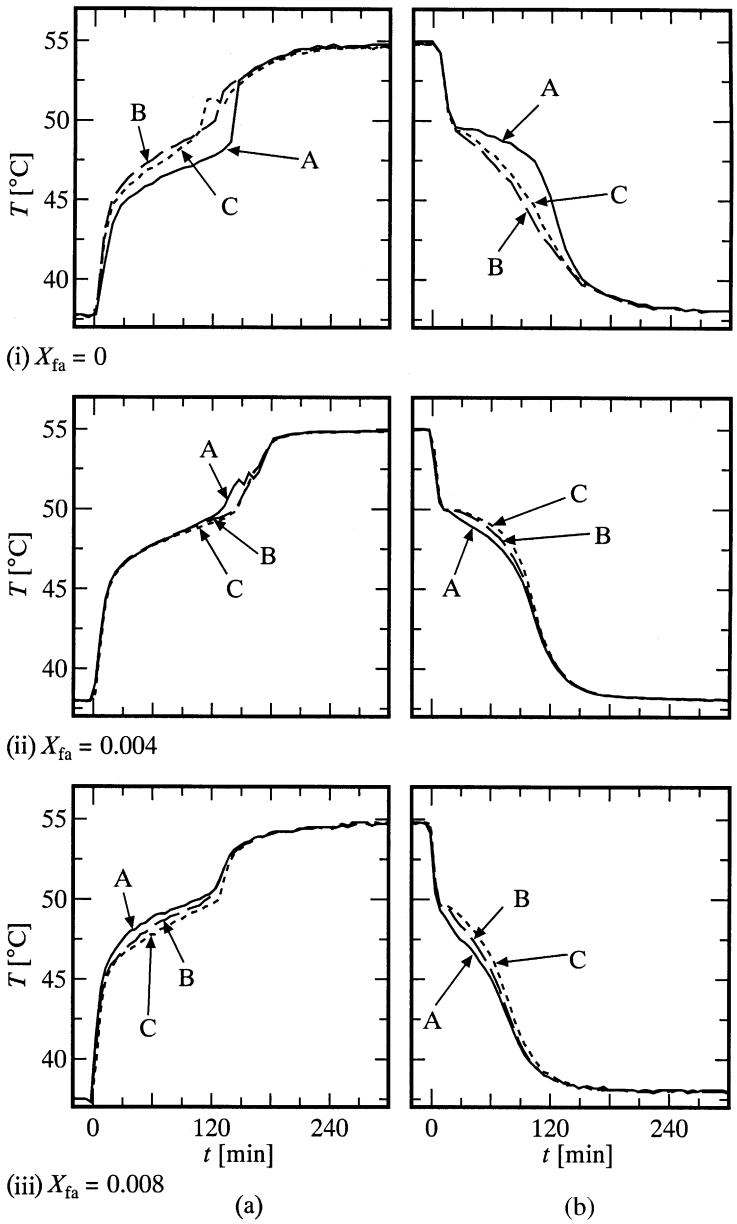

Fig. 6. The time variations in the experimental local temperatures in the brush/PCM composite ($u_h = 0.03$ m/s). (a) Charge and (b) discharge.

present model almost predicts the time variation in the local temperatures.

5. Conclusion

A shell-and-tube type heat exchanger is used to store latent heat thermal energy. The special feature of this thermal storage unit is the insertion of carbon-fiber brushes for enhancing the conductive heat transfer rate in the PCMs. The effect of the brush on the thermal responses of the unit has been experimentally and numerically investigated. The summary is described below:

(1) In the discharge process, the discharge rate using the brushes with one volume percent is about 30% higher than that using no fibers.

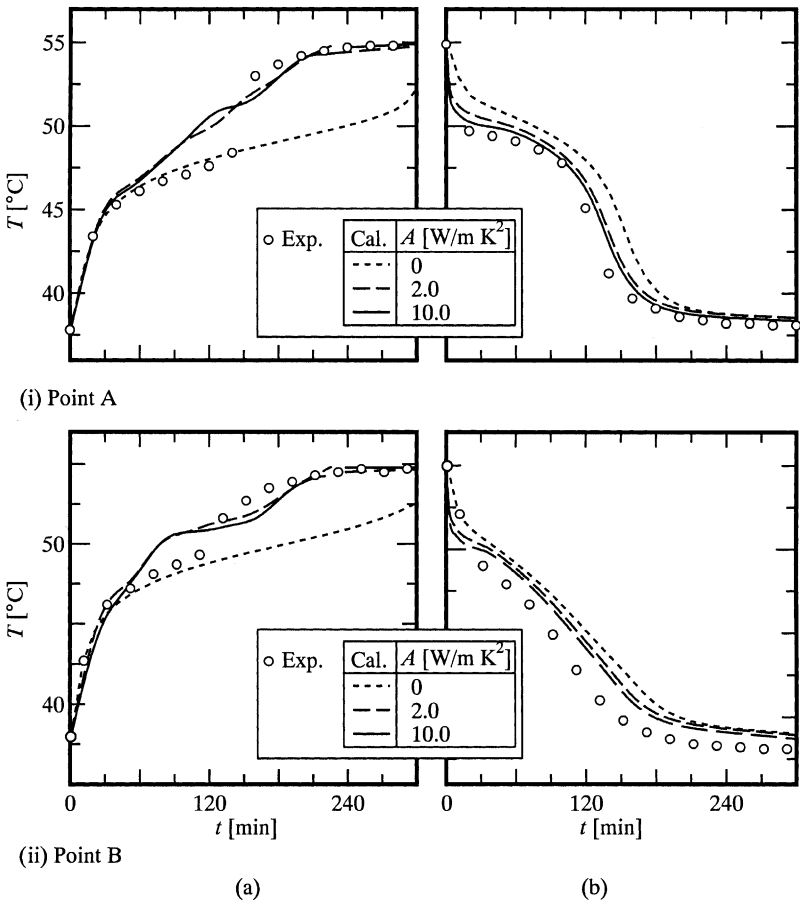

Fig. 7. The effect of the A-value on the calculated local temperatures in the PCM ($X_{fa} = 0$, $u_h = 0.03$ m/s). (a) Charge and (b) discharge.

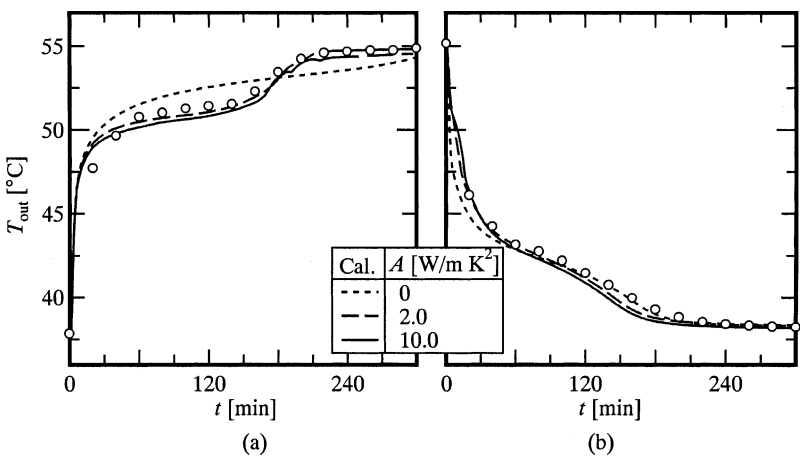

Fig. 8. The effect of the A-value on the calculated outlet fluid temperature (open circle: experiment, $X_{fa} = 0$, $u_h = 0.03$ m/s). (a) Charge and (b) discharge.

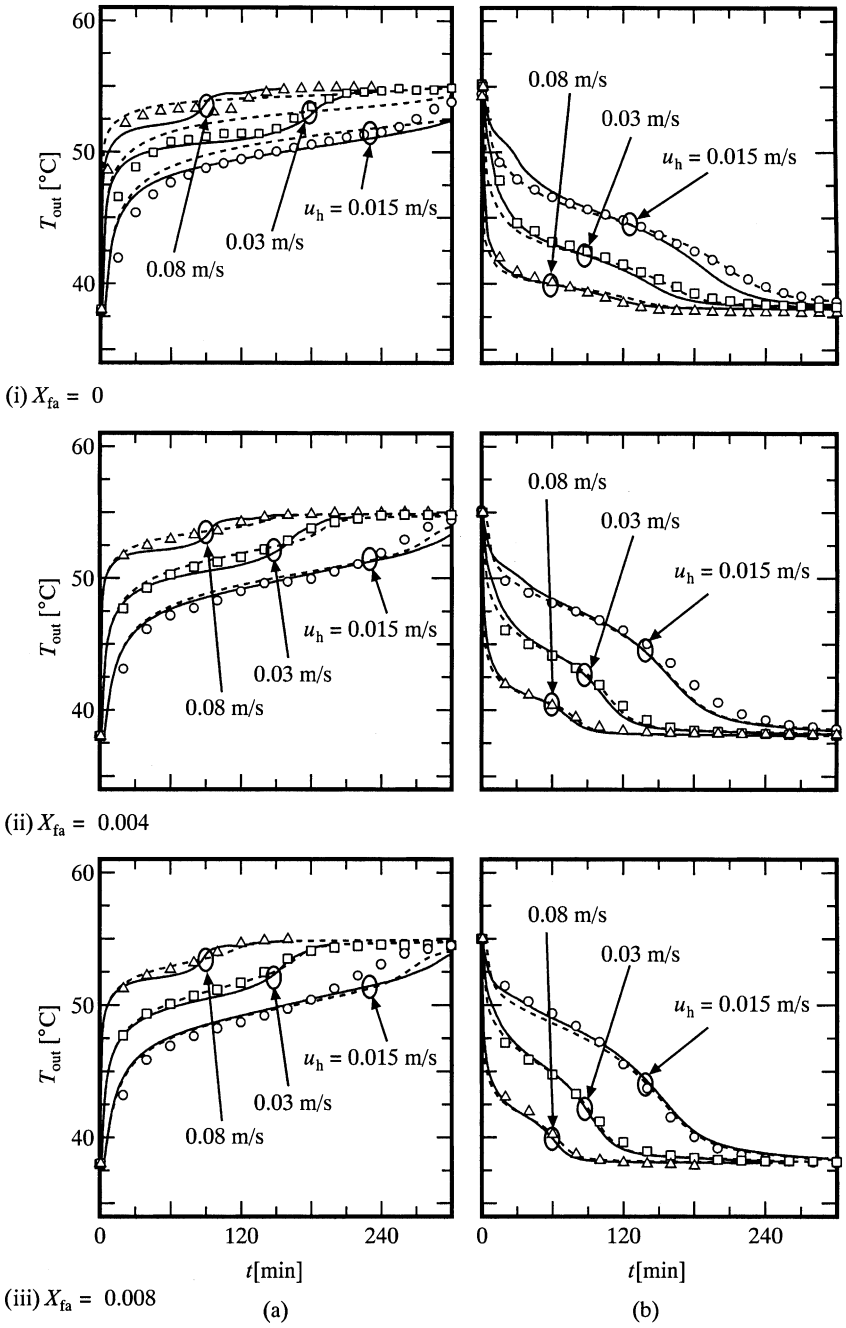

Fig. 9. The effect of the A-value on the outlet fluid temperature (dotted curves: $A = 0$ W/m K^2, solid curves: $A = 2$ W/m K^2). (a) Charge and (b) discharge.

(2) In the charge process, the brushes prevent the natural convection. However, the charge rate with the brushes is 10–20% higher than that with no fiber. Accordingly, an increase in the effective thermal conductivity fully makes up for the reduction in the convective heat transfer rate.

(3) The two-dimensional simple model previously reported is extended to describe the three-dimensional heat transfer in the thermal energy storage unit.

(4) When the brushes are added, the developed model predicts well the outlet fluid temperature under various experimental conditions.

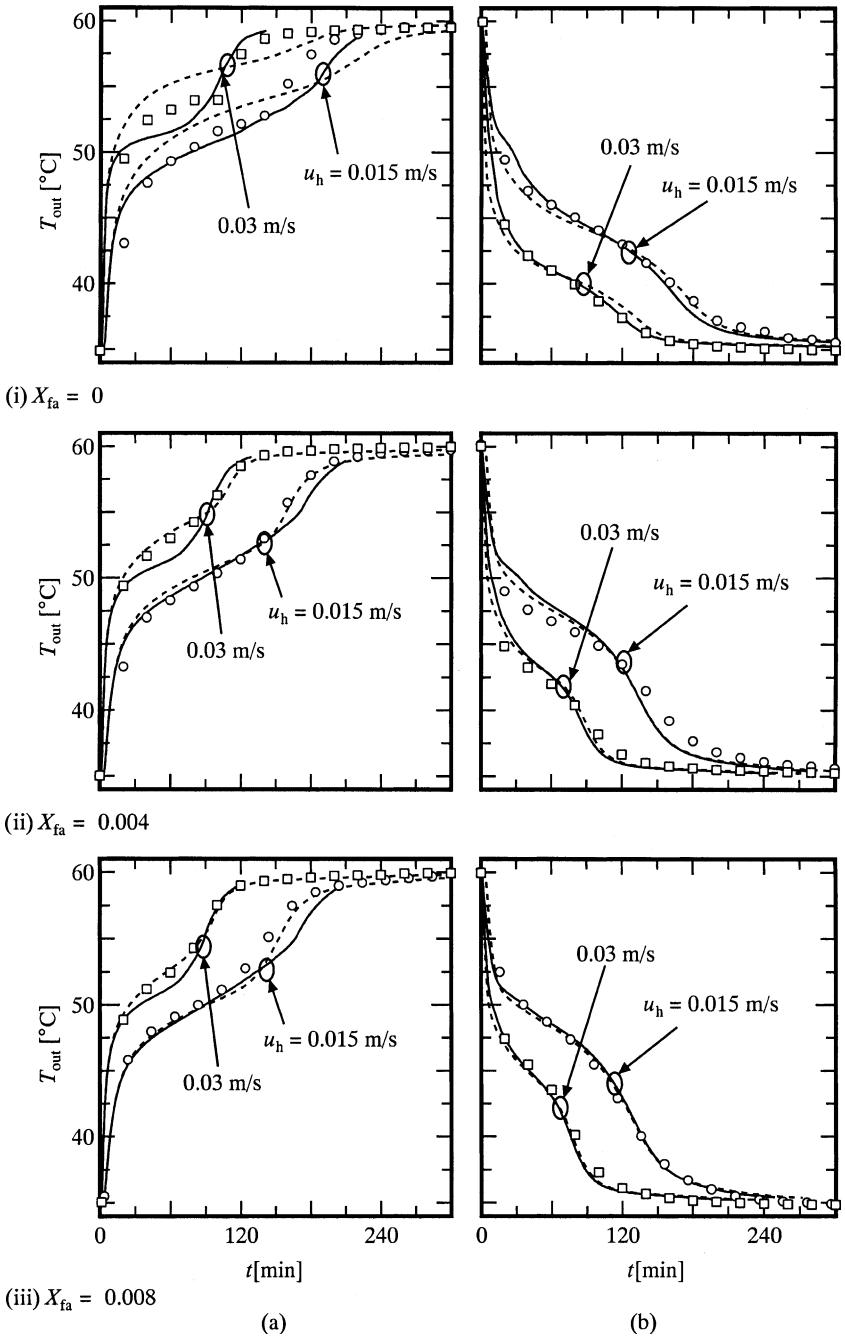

Fig. 10. The effect of the A-value on the outlet fluid temperature (dotted curves: $A = 0$ W/m K^2, solid curves: $A = 2$ W/m K^2). (a) Charge and (b) discharge.

(5) When the brushes are not added, the developed model predicts well the outlet fluid temperature by assuming high thermal conductivities in the liquid phase.
(6) It should be noted that there is no fitting parameter in the present model. Although several empirical constants are included in Eqs. (14)–(16), their values have been identified on the basis of the experimental and theoretical investigations using another experimental setup and are applicable into laboratory-scale apparatuses to practical-scale ones [19].

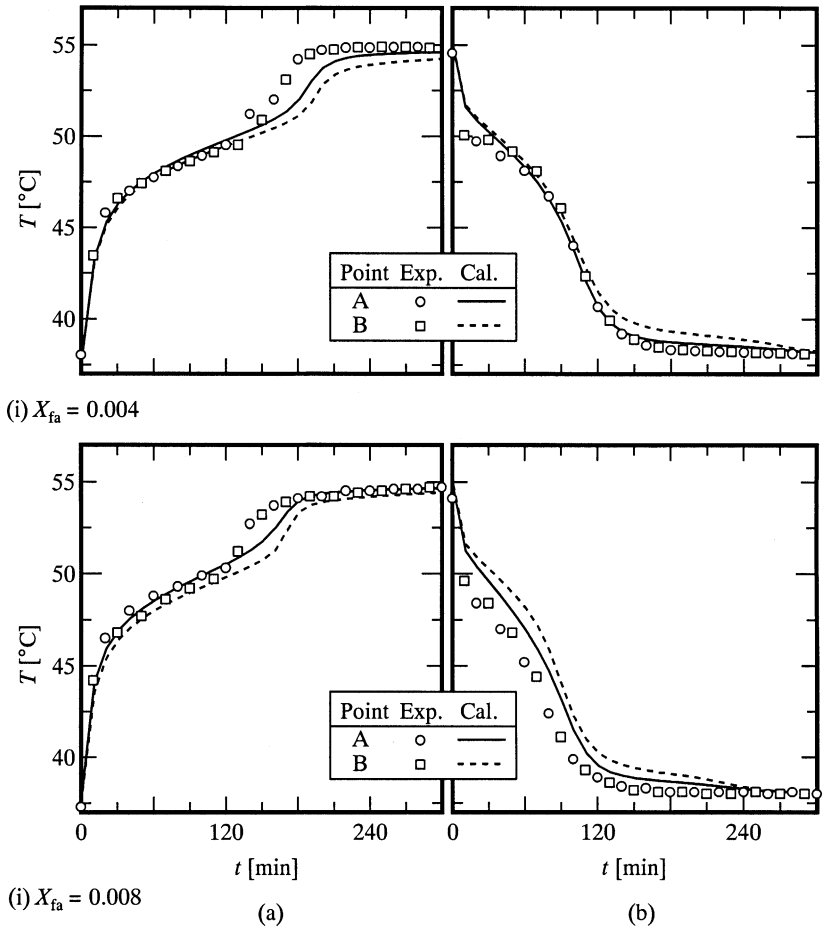

Fig. 11. The effect of A-value on the calculated local temperatures ($u_h = 0.03$ m/s, $A = 0$ W/m K^2). (a) Charge and (b) discharge.

References

[1] S.M. Hasnain, Review on sustainable thermal energy storage technologies, Part I: heat storage materials and techniques, Energy Convers. Manage. 39 (1998) 1127–1138.

[2] D.E. Beasley, C. Ramanarayanan, H. Torab, Thermal response of a packed bed of spheres containing a phase-change material, Int. J. Energy Res. 13 (1989) 253–256.

[3] J.P. Bedecarrats, F. Strub, B. Falcon, P. Dumas, Phase-change thermal energy storage using spherical capsules: performance of a test plant, Int. J. Refrigerat. 19 (1996) 187–196.

[4] J. Fukai, H. Omori, A. Oishi, O. Miyatake, Effect of carbon fibers on thermal response within heat storage material, Kagaku Kogaku Ronbun. 23 (1997) 82–87.

[5] K. Cho, S.H. Choi, Thermal characteristics of paraffin in a spherical capsule during freezing and melting processes, Int. J. Heat Mass Transfer 43 (2000) 3183–3196.

[6] J. Fukai, A. Oishi, H. Omori, M. Kanou, Y. Kodama, O. Miyatake, Discharge characteristics of capsule-type thermal energy storage unit using carbon-fiber/paraffin composite, Kagaku Kogaku Ronbun. 26 (2000) 119–121.

[7] J. Wang, Y. Ouyang, G. Chen, Experimental study on charging processes of a cylindrical heat storage capsule employing multiple-phase-change materials, Int. J. Energy Res. 25 (2001) 439–447.

[8] Y. Zhang, Y. Su, Y. Zhu, X. Hu, A general model for analyzing the thermal performance of the heat charging and discharging processes of latent heat thermal energy storage systems, Trans. ASME 123 (2001) 232–236.

[9] X. Py, R. Olives, S. Mauran, Paraffin/porous-graphite-matrix composite as a high and constant power thermal storage material, Int. J. Heat Mass Transfer 44 (2001) 2727–2737.

[10] A.G. De Jong, C.J. Hoogendoorn, Improvement of heat transport in paraffines for latent heat storage systems, Therm. Storage Solar Energy (1981) 123–133.

[11] K. Sasaguchi, H. Imura, H. Furusho, Heat transfer characteristics of latent heat storage unit with a finned tube, Bull. JSME 29 (1986) 2986–2992.

[12] M. Lacroix, Study of the heat transfer behavior of a latent heat thermal energy storage unit with a finned tube, Int. J. Heat Mass Transfer 36 (1993) 2083–2092.

[13] Y. Zhang, A. Faghri, Heat transfer enhancement in latent heat thermal energy storage system by using an external radial finned tube, J. Enhanc. Heat Transfer 3 (1996) 119–127.
[14] K.A.R. Ismail, C.L.F. Alves, M.S. Modesto, Numerical and experimental study on the solidification of PCM around a vertical axially finned isothermal cylinder, Appl. Therm. Eng. 21 (2001) 53–77.
[15] S.M. Hasnain, B.M. Gibbs, Effect of extended surfaces in a solar energy storage unit, in: Proceedings of the 2nd U.K. National Conference on Heat Transfer of U.K. (1988) 833–844.
[16] C.J. Hoogendoorn, G.C.J. Bart, Performance and modeling of latent heat stores, Energy 48 (1992) 53–58.
[17] O. Nomura, K. Tanaka, Y. Abe, Y. Takahashi, K. Kanari, M. Kamimoto, Heat transfer experiments on latent thermal storage units using composite materials for space solar dynamic power systems, Space Power 12 (1993) 229–253.
[18] J. Fukai, M. Kanou, Y. Kodama, O. Miyatake, Thermal conductivity enhancement of energy storage media using carbon fibers, Energy Convers. Manage. 41 (2000) 1543–1556.
[19] J. Fukai, Y. Hamada, Y. Morozumi, O. Miyatake, Effect of carbon-fiber brushes on conductive heat transfer in phase change materials, Int. J. Heat Mass Transfer 45 (2002) 4781–4792.
[20] S.V. Patankar, Numerical Heat Transfer and Fluid Flow, McGraw-Hill, New York, 1980.